Article:
Senatore, EV, Pinto, MCP, Souza, EA et al. (2021) Effects of pre-filmed FeCO3 on flow-induced corrosion and erosion-corrosion in the absence and presence of corrosion inhibitor at 60 °C. Wear, 480-481. 203927. ISSN: 0043-1648

https://doi.org/10.1016/j.wear.2021.203927

EFFECTS OF PRE-FILMED $FeCO_3$ ON FLOW-INDUCED CORROSION AND EROSION-CORROSION IN THE ABSENCE AND PRESENCE OF CORROSION INHIBITOR AT 60ºC

E. V. Senatore[1], M.C.P. Pinto[1], E.A.Souza[1], R. Barker[2], A. Neville[2], J. A. C. Ponciano Gomes[1]

[1]Federal University of Rio de Janeiro-LabCorr, Rio de Janeiro, Brazil

[2]University of Leeds, Leeds, United Kingdom

ABSTRACT

In CO_2 environments, an increase in the temperature can influence carbon steel flow-induced corrosion (FIC) and erosion-corrosion (EC) degradation processes. Increasing temperature typically results in the acceleration of electrochemical degradation mechanisms in the absence of protective corrosion product layers. Furthermore, the presence of sand in corrosive process fluids could aggravate the service conditions. Although protective iron carbonate ($FeCO_3$) film or/and corrosion inhibitors are capable of suppressing corrosion in CO_2-containing environments typical of oil and gas production, their ability to suppress degradation and their associated mechanisms in erosion-corrosion environments is less understood. This work focuses on understanding the ability of $FeCO_3$ to protect the steel surface in the absence and presence of corrosion inhibitor and their interactions in flow-induced and erosion-corrosion systems at 60°C. The effect of the temperature increase is investigated based on results obtained in a previous study performed at 25°C. $FeCO_3$ filmed carbon steel specimens were developed using an autoclave at 60°C, pH 6.6 and 30bar in a 1.5 wt.% NaCl CO_2-saturated solution over 48h. The $FeCO_3$ covered specimens were evaluated in FIC and EC environments at 60°C and a flow velocity of 15 m/s in the presence and absence of 1000 mg/L sand and 100 ppm of a commercially available corrosion inhibitor. Results indicate that the sole presence of an $FeCO_3$ layer is not sufficient to retard the corrosive process of carbon steel at 60°C under EC conditions. However, the commercial corrosion inhibitor was observed to worked synergistically with the $FeCO_3$ layer to reduce the corrosion degradation component in both the presence and absence of sand particles. The erosion component is also reduced in erosion-corrosion environments as a result of the combined presence of $FeCO_3$ and corrosion inhibitor.

Keywords: flow-induced corrosion, erosion-corrosion, CO_2 corrosion, protective layer, corrosion inhibitor, carbon steel

1 INTRODUCTION

The control of carbon steel carbon dioxide (CO_2) corrosion presents a significant challenge within the petroleum industry as the materials used in transport pipelines are often exposed to corrosive environments containing this gas [1]. CO_2 is soluble in water and in liquid hydrocarbons. In multiphase environments, the presence of CO_2 increases the complexity of the corrosion process, since CO_2 partitioning between water and organic phases can cause high corrosion rates [2].

Furthermore, sand is commonly produced along with production fluids and the presence of solid particles in the corrosive environment can enhance the degradation process due to the contribution of mechanical erosion [3,4]. The combination of mechanical removal and electrochemical dissolution is defined as erosion-corrosion. The mass loss associated with this mechanism can significantly exceed the sum of partial components of pure corrosion and pure erosion as a result of the synergic interaction between erosion and corrosion [3, 5-8]. This regime of degradation is becoming more common due to increased sand production and the increasing severity of conditions attributed to extracting oil from ageing and deeper wells [6]. Consequently, investigation of combined erosion and corrosion processes is necessary to provide the basic knowledge necessary to prevent or mitigate this severe deterioration process.

Many previous studies have evaluated the erosion-corrosion resistance of carbon steel in CO_2-containing environments [5, 9-13]. These authors reported that erosion-corrosion mechanism is complex and extensive research has been conducted to investigate the interaction between corrosion and erosion degradation components. Furthermore, they have demonstrated that corrosion inhibitors can prevent not only steel dissolution in environments containing CO_2, but can alleviate and reduce the impact of the erosion component [14].

Corrosion inhibitors are common methods for controlling corrosion and erosion-corrosion of carbon steels. The efficiency of this technology is affected by different parameters, including environment temperature, inhibitor concentration used, flow velocity, sand erosion intensity, presence of metal cations, chlorides concentration, metal characteristics, pH, system geometry, among other factors [12]. According to literature, inhibitors can interact with internal pipeline metallic surface and the sand particles, depending on their affinity for each surface [13]. In instances where the corrosion inhibitor is adsorbed onto the surface of sand particles, there is a reduction of the bulk inhibitor concentration which influences the adsorption onto the steel surface. The capability of these chemicals to lower electrochemical corrosion reactions and the

mechanical damage associated with particle impingement is well documented, but the underlying mechanisms deserves further investigation [5,15] since an inhibitor that is superior under static or low flow rate conditions may be not suitable in high flowing conditions due to shear stress [16].

Beyond that, corrosion products formed in CO_2-containing environments are deposited on the internal pipeline surface and it is well known that the corrosion rates can be significantly reduced [11, 17, 18]. Under specific conditions, an iron carbonate ($FeCO_3$) corrosion product layer can be formed on the steel surface by precipitation when the activities of Fe^{2+} and CO_3^{2-} ions exceed the solubility limit, which is a function of temperature [19]. The thickness of this $FeCO_3$ layer can achieve orders of 10's or 100's µm and the protection under erosion-corrosion conditions will depend on the ability to outstand the erosive effect promoted by sand particle impingement [9].

Some researchers have investigated the interaction between corrosion products and inhibitors [7, 9, 19, 20]. They identified that some properties of corrosion layers, such as thickness and intrinsic growth induced residual stress can be reduced when one inhibitor is introduced into the system. Furthermore, the performance of the inhibitor can be impaired if introduced when pre-corroded surfaces, containing corrosion product layers, are present [7]. According to Choksi et al. [21], the presence of inhibitors can decrease the $FeCO_3$ film growth rate due to the lowering of Fe^{2+} concentration at the metal-electrolyte interface.

The present work focuses on the assessment of the protection promoted by $FeCO_3$ corrosion product, on API 5L X65 carbon steel substrates in CO_2-containing environment, under flow induced corrosion and erosion-corrosion conditions. The investigation was conducted in environments in the absence and presence of a commercial corrosion inhibitor. Erosion was produced by the impingement of sand particles. Effects of temperature on the stability of the corrosion product layer formed by precipitation was investigated.

2 METHODOLOGY

The material used in this study is an API 5 L X65 carbon steel commonly employed in the oil and gas industry due to its adequate mechanical properties and low cost. The steel possesses a ferritic/pearlitic microstructure and the elemental composition is C: 0.12, Mn: 1.27, Si: 0.18, P: 0.008, S: 0.002, Ni: 0.07, Cr: 0.11, Mo: 0.17, Cu: 0.12, Sn: 0.008, Al: 0.022, B: 0.0005, Nb: 0.054, Ti: 0.001, V: 0.057 and Fe balanced.

2.1 SAMPLE PREPARATION

The test specimens used in this work were discs with an exposed area of 4.9 cm^2 (25 mm diameter specimens) for electrochemical, mass loss measurements and further surface analysis. Two different steel surface conditions were considered to perform the FIC and EC tests.

The first surface condition consisted of wet-grinding the sample using 1200 grit silicon carbide abrasive paper before degreasing with acetone, followed by high purity ethanol and drying with compressed air. The second surface condition was the steel sample covered by an $FeCO_3$ film layer previously generated in a CO_2-saturated 1.5 wt.% NaCl solution at 60ºC and 30 bar and pH adjusted to 6.6 in an autoclave during 48 hours

2.2 TESTS PERFORMED

2.2.1. FLOW INDUCED CORROSION (FIC) AND EROSION CORROSION (EC) TESTS

Flow Induced Corrosion and Erosion Corrosion tests were performed on a Submerged Impingement Jet (SIJ) equipment, which is one of the most commonly used for erosion-corrosion testing as a method of quantifying each of contributing factors to total erosion-corrosion degradation at high flow velocity across a range of temperatures, sand particle impact angles and brine chemistries. Figure 1 shows the schematic drawing of the SIJ apparatus used in this study.

The system consists of two reservoirs with a 70-litre capacity which relate to a storage tank and a test tank. This test rig is similar to the one previously used [9], modified by the introduction by the second tank. The presence of two tanks reduced the contamination of the system by oxygen (O_2) since the solution and the test specimens were placed in the tank and are sealed before the test started. The other test parameters were the same used for room temperature tests [9].

Before starting FIC and EC tests, the SIJ rig was calibrated in order to control the flow velocity based on the parameters pump frequency and solid particles concentration.

Test procedure is described as follows. Prior to each test, the 3.5 wt.%NaCl solution was saturated with CO_2 in the fully sealed storage tank. At the same time, the test specimens were positioned in holders at a 90° flow incidence angle in the test tank which was also sealed and saturated with CO_2. After the saturation time previously

established, the solution was transferred to the test tank and was continuously sparged with CO_2 throughout the entire experiment, preventing the entrance of O_2 into the system. The diameter of each nozzle used was 4mm and was position 5 mm from the steel specimen surface.

Instrumentation to obtain pH and dissolved O_2 measurements were coupled in a transfer cell, containing a small amount of the solution to perform the measurements throughout the CO_2 saturation period. Therefore, it was possible to control these parameters before starting each test, as can be observed in Figure 2. After approximately 50h of CO_2 bubbling, the pH values close to 3.8 were achieved, while the dissolved O_2 was reduced to below 0.07 ppm, as expected from the design of the system with two tanks.

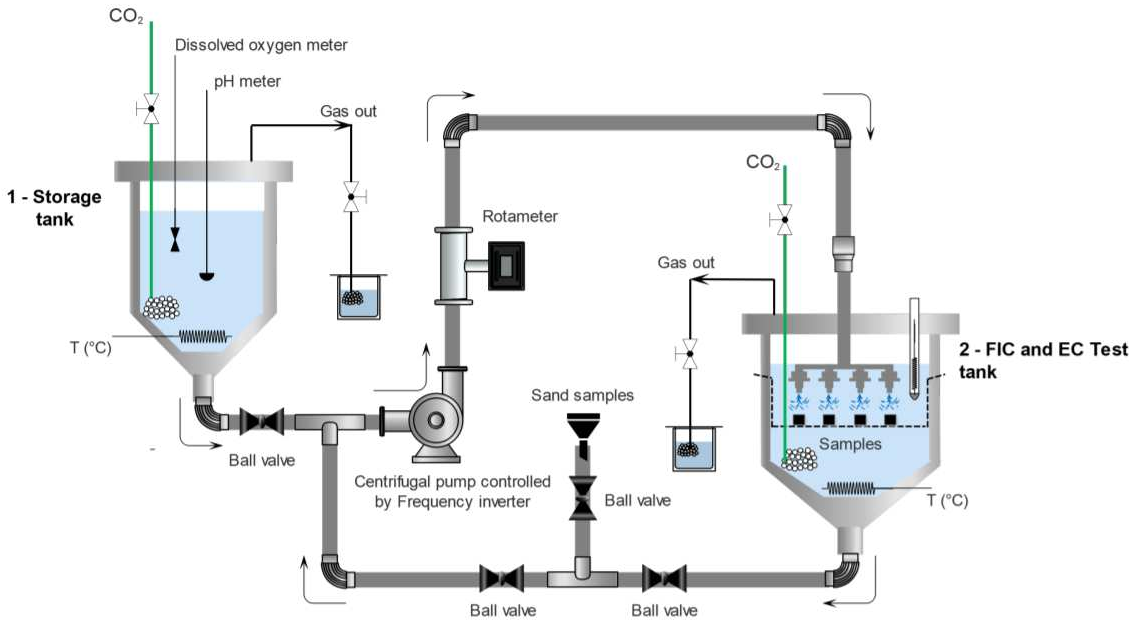

Figure 1: Schematic drawing of SIJ equipment used for Flow-Induced corrosion and Erosion-Corrosion tests

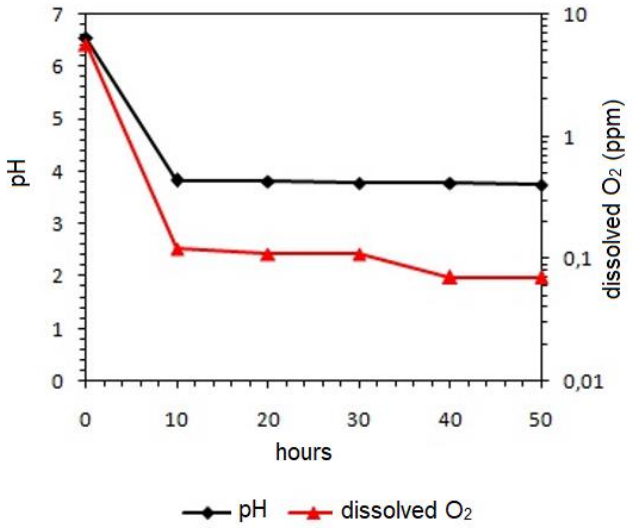

Figure 2: pH and dissolved O_2 during CO_2 saturating time in a 3.5wt% NaCl solution at 60°C in the SIJ.

FIC tests were conducted in SIJ equipment (Figure 1) using 3.5 wt.% NaCl solution saturated with CO_2 at a flow velocity of 15 m/s and at 60°C. In these tests, the brine solution is recirculated in the jet impingement system, reaching the surface of the test specimen at a 90° angle. The purpose of these tests was to evaluate the corrosion component in a flow system through the use of electrochemical measurements.

For EC tests, the same conditions as FIC tests were used, in the presence of solid particles introduced into the system. The concentration of sand particles was 1000 mg/L and the average diameter was 250 μm [9]. Sand was added to the system after the pump was started to ensure a homogeneous distribution throughout the rig. The mixture of brine solution and solid particles were recirculated in the SIJ system. The purpose of these tests was to analyse the joint influence of corrosion and mechanical erosion due to the impact of the particles on the metal surface. For this, both electrochemical and gravimetric measurements were used.

In order to establish whether the effects of degradation in both FIC and EC environments could be sufficiently suppressed, a commercial high shear CO_2 corrosion inhibitor based on a combination of 2-butoxyethanol, quaternary ammonium compounds and amines was used. This chemical was also used in previous work at 100 ppm [9] at room temperature. The summary of the experimental conditions is shown in Table 1.

Table 1: Summary of test conditions – Constant temperature of 60°C

EC: Erosion Corrosion; FIC: Flow Induced Corrosion

TEST CONDITION	Inhibitor Concentration (ppm)	Sand particles concentration (mg/L)	Surface condition	Corrosion Process
A	0	0	Wet Ground	FIC
B	0	1000	Wet Ground	EC
C	100	0	Wet Ground	FIC
D	100	1000	Wet Ground	EC
E	0	0	$FeCO_3$	FIC
F	0	1000	$FeCO_3$	EC
G	100	0	$FeCO_3$	FIC
H	100	1000	$FeCO_3$	EC

Prior to FIC and EC tests with $FeCO_3$ pre-filmed on surface (Conditions E, F, G, H), static tests were carried (60°C and 3.5 wt.% NaCl) in order to assess, without the influence of flow and solid particles, the persistence of the iron carbonate film ($FeCO_3$) and its possible interference on performance of the corrosion inhibitor in long-term tests (45h).

2.3 DEGRADATION RATE ASSESSMENT

The API 5L X65 steel degradation rate was quantified by using mass loss and electrochemical measurements.

Mass loss measurements were conducted on EC samples while electrochemical measurements were performed on both EC and FIC samples. After 6 h of exposure, the mass loss samples were removed from the rig, cleaned with Clarke solution (20 g antimony trioxide + 50 g stannous chloride + 1000 ml 38% hydrochloric acid) in accordance with ASTM Standard G1–03, rinsed with distilled water, dried with compressed air and weighed to determine the mass loss. Then, the corrosion rate (mm/year) from mass loss measurements can be calculated by the following equation [22].

$$CR = \frac{K.M}{A.t.\rho} \qquad \text{Equation 1}$$

where K is a constant (8.76×10^{-4}), M is the mass loss (g), A is the area (cm^2), t is the time of exposure (h) and ρ is the density ($g.cm^{-3}$)

Electrochemical measurements involved the use of the Linear Polarisation Resistance (LPR) technique which was implemented to provide a general corrosion rate

across the entire steel surface. The SIJ was integrated with a three-electrode cell which comprised of a working electrode, a platinum auxiliary electrode and Ag/AgCl reference electrode (Figure 3). Linear polarisation resistance (LPR) measurements were performed using a voltage of ± 15mV relative to the Open Circuit Potential (OCP) was applied with a scan rate of 0.333 mV/s.

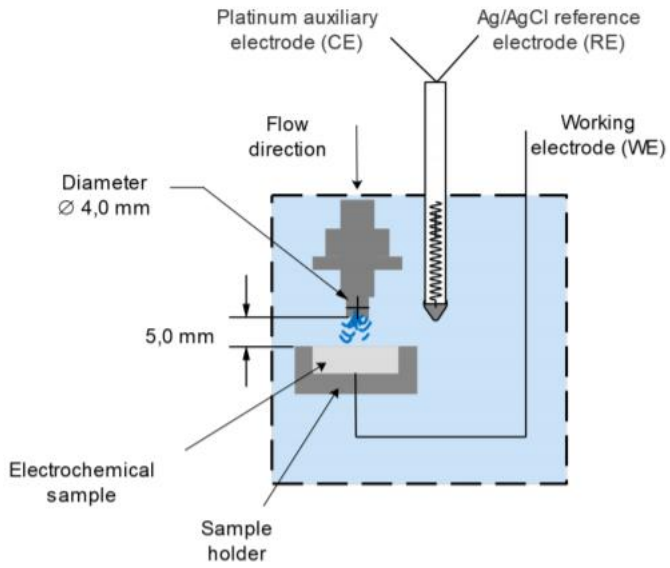

Figure 3: Schematic drawing of three-electrode cell which comprised of a working electrode, a platinum auxiliary electrode and Ag/AgCl reference electrode integrated within SIJ equipment.

A Metrohm® AUTOLAB - PGSTAT 302N potentiostat/galvanostat was used to the acquisition and processing of the electrochemical results.

A script routine runs according to the following steps for FIC and EC tests:

I. 10 min for OCP stabilization;

II. LPR over 4.5 hours

A script routine runs according to the following steps for complementary static tests:

I. 10 min for OCP stabilization;

II. LPR over 45 hours

The polarization resistance obtained from the LPR measurements was adjusted based on the solution resistance (determined from impedance measurements) resulting in a charge transfer resistance (R_{ct}) value. This resistance was converted into a corrosion

rate through the application of the Stern-Geary ratio (using Tafel's anodic and cathodic inclinations) and Faraday's Law (Equations 2 to 4) [23].

$$B = \frac{\beta_a \beta_c}{2.303\,(\beta_a+\beta_c)} \qquad \text{Equation 2}$$

$$i_{corr} = \frac{\beta_a \beta_c}{2.303\,R_{ct}\,(\beta_a+\beta_c)} \qquad \text{Equation 3}$$

$$CR = \frac{3.27 i_{corr} EW}{\rho} \qquad \text{Equation 4}$$

where B is the Stern-Geary coefficient, β_a is the anodic Tafel constant (V), β_c is the cathodic Tafel constant (V), i_{corr} is the corrosion current density ($mA.cm^{-2}$). CR is the corrosion rate (mm/year), 3.27 is a conversion factor, EW is the equivalent weight of steel (equal to the molecular weight of steel (55.847 g/mol) divided by the number of electrons involved in the corrosion process (2) and ρ is the steel density ($g.cm^{-3}$)

2.4 TOTAL DEGRADATION RATE

The Total Mass Loss (TML) values expressed for the tests can be attributed to the summation of four different material loss components [13] as shown in Equation 5:

$$TML = E + C + dE_C + dC_E \qquad \text{Equation 5}$$

where TML is the total mass loss, E is pure erosion in the absence of corrosion and C is the corrosion in the absence of erosion, dC_E is the effect of erosion on corrosion and dE_C is the effect of corrosion on erosion [13]. The combination of dE_C and dC_E is termed as the synergistic effect which is the factor responsible for producing degradation rates higher than the summation of the erosion and corrosion rates acting individually.

From the data collected in E-C conditions, it is possible to determine the contribution of the corrosion component ($C+dC_E$) through the application of in situ electrochemistry and the erosion component (E+dEc) using the total mass loss in conjunction with the corrosion component.

2.5 SURFACE ANALYSIS

Scanning electron microscopy (SEM) was performed to determine the characteristics of the corrosion products formed on the steel surface and the morphology

of wear degradation after SIJ tests. Taylor Hobson Talysurf 2D was also used after tests to characterise the steel surface morphology produced by the impacts of sand particles.

3 RESULTS AND DISCUSSION

3.1. FIC AND EC TESTS OF WET-GROUND X65 STEEL SPECIMENS – TEST CONDITIONS A, B, C, D

3.1.1. ELECTROCHEMICAL RESULTS

FIC and EC tests were performed at 60°C in the presence and absence of corrosion inhibitor. No iron carbonate film ($FeCO_3$) is previously formed on surface of test samples and no iron carbonate film formation was observed on sample surface during FIC and EC tests and it could be confirmed in SEM imagens (section 3.1.3). Although the test temperature (60ºC) is favourable to iron carbonate film precipitation due to decrease the solubility limit, the ratio volume/area (V/A ~ 3572 cm), where V is the volume of solution and A is the total area of steel exposed to the environment, is too high, making this precipitation difficult during these experimental conditions.

Table 2 presents the Stern-Geary coefficients (B) applied for the calculation of corrosion rate using the LPR data. The analysis of LPR results and its representation could be seen in Figure 4, which compares the corrosion rates for FIC and EC conditions at 60°C in the presence and absence of corrosion inhibitor.

Table 2: Stern-Geary coefficients used in Flow Induced Corrosion and Erosion Corrosion tests.

	FIC 60ºC Blank	FIC 60ºC Inhibitor	EC 60°C Blank	EC 60ºC Inhibitor
βa (mV/decade)	100	67	101	65
βc (mV/decade)	126	325	128	202
Stern-Geary coefficient (B) mV/decade	23.17	24.08	24.45	21.36

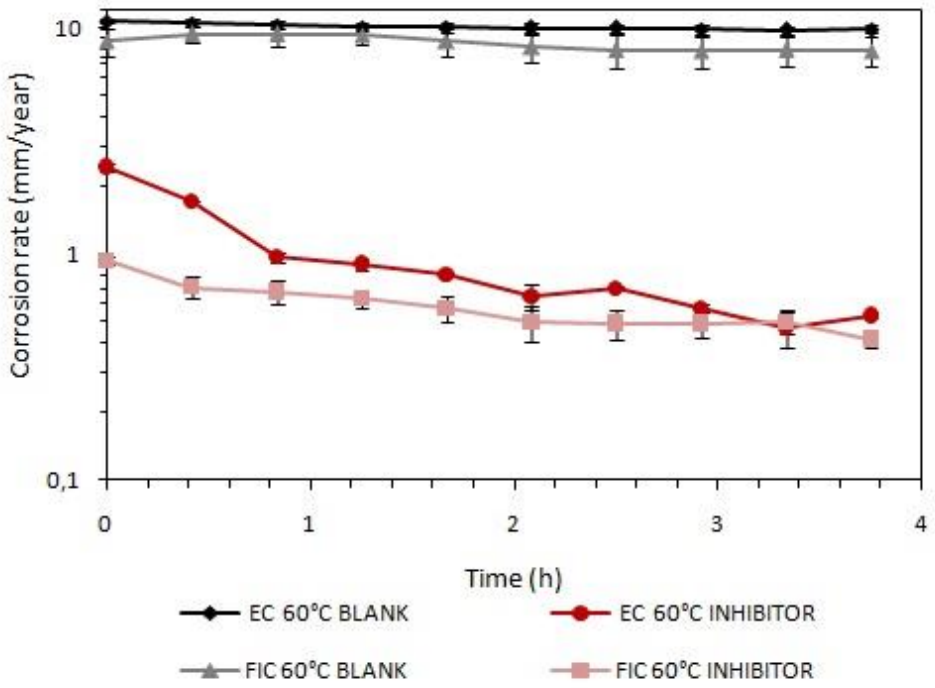

Figure 4: Corrosion rates obtained from LPR measurements in FIC and EC tests with and without corrosion inhibitor on wet-ground X65 steel specimens. Test conditions: 3.5wt.% NaCl, 15 m/s, 60°C, 0 or 1000 mg/L of sand and 0 or 100 ppm inhibitor.

For the FIC tests, the corrosion rates under uninhibited conditions (blank tests condition) presented a value close to 8.0 mm/year at the end of the experiment and it represents almost twice the value (4.9 mm/year) obtained at 25°C in similar conditions [9]. Referring to Figure 4, it is clear that the inhibitor is effective in reducing corrosion rate at 60°C. With the introduction of 100 ppm of corrosion inhibitor, the corrosion rate was reduced from 8.0 mm/year to values close to 0.4 mm/year and it represents an electrochemical efficiency of inhibitor of approximately 95% for the tests carried out with no sand particles. Comparing this electrochemical efficiency at 60°C with an obtained at 25°C [9], it is possible to observe that damage associated to corrosion can be decreased by 95% and 98%, respectively, showing that this inhibitor does not lose its efficiency at higher temperatures when no presence of sand erosive.

In EC tests (1000 mg/L), the presence of corrosion inhibitor also reduces the corrosion rate (electrochemical component). It can be seen that the corrosion rate decreased from 9.9 to 0.5 mm/year, that is, electrochemical efficiency of inhibitor of 95%. Comparing this efficiency with obtained at 25°C (96%) [9], it was possible to identify that the use of 100 ppm of inhibitor is able to reduce significantly corrosion rate and its electrochemical efficiency is maintained regardless of whether test temperature.

Table 3 summarize the corrosion rates obtained by LPR electrochemical technique at 25°C [9] and 60°C.

Table 3: Corrosion Rate obtained from LPR at 25 [9] and 60°C

Test conditions		Corrosion rate (mm/year) versus Temperature (°C)	
		25°C [9]	60°C [current paper]
FIC	0 ppm inhibitor (blank)	4.9	8.0
	100 ppm inhibitor	0.08	0.4
EC	0 ppm inhibitor (blank)	5.5	9.9
	100 ppm inhibitor	0.2	0.5

The higher temperature accelerates all the processes involved in corrosion: electrochemical, chemical and species transport. One would expect then that the corrosion rate increases with temperature, and this is the case at low pH when precipitation of $FeCO_3$ or other protective scales does not occur [24]. No $FeCO_3$ formation was observed on sample surface during these tests. Furthermore, the carrier fluid viscosity decreases, leading to an increase in the Reynolds number, turbulence and particle velocity and consequently, the level of erosion tends to increase [25] and it will be confirmed by gravimetric results and SEM analysis.

Although the almost constant efficiency, the absolute corrosion rate values are higher during the entire test associated with the sand impingement onto the metal surface, which causes periodic removal of the inhibitor film, exposing the specimen surface to the aggressive environment. However, it must be emphasised that this inhibitor efficiency is associated with the electrochemical component, and does not include the erosion effects.

Beyond that, according to literature, the total inhibitor efficiency could be reduced because of the presence of active compounds within the inhibitor that adhere to the sand particles and reduce the inhibitor concentration in the bulk solution [15]. However, in this study, it was possible to observe that the effect of the inhibitor on the corrosion component did not present a variation with the introduction of the sand. It is important to highlight that the total efficiency of inhibitor in EC test must be associated to reduction in a Total Mass Loss (TML), that is related to sum of erosion and corrosion contributions.

3.1.2. TOTAL DEGRADATION RATE

The contribution of the corrosion and the erosion components in the total degradation is presented in Table 4 and Figure 5 in the presence and absence of 100 ppm corrosion inhibitor. It is important to emphasize that the surface area exposed to the corrosive environment in gravimetric tests was the same used in electrochemical tests.

Table 4: Contribution of erosion and corrosion components of degradation

Test conditions		Mass loss (mg) associated to components of degradation		
		C + dCe	E + dEc	TML
FIC	0 ppm inhibitor (blank)	21.10	-	21.10
	100 ppm inhibitor	1.06	-	1.06
EC	0 ppm inhibitor (blank)	26.28	13.87	40.15
	100 ppm inhibitor	1.69	7.21	8.90

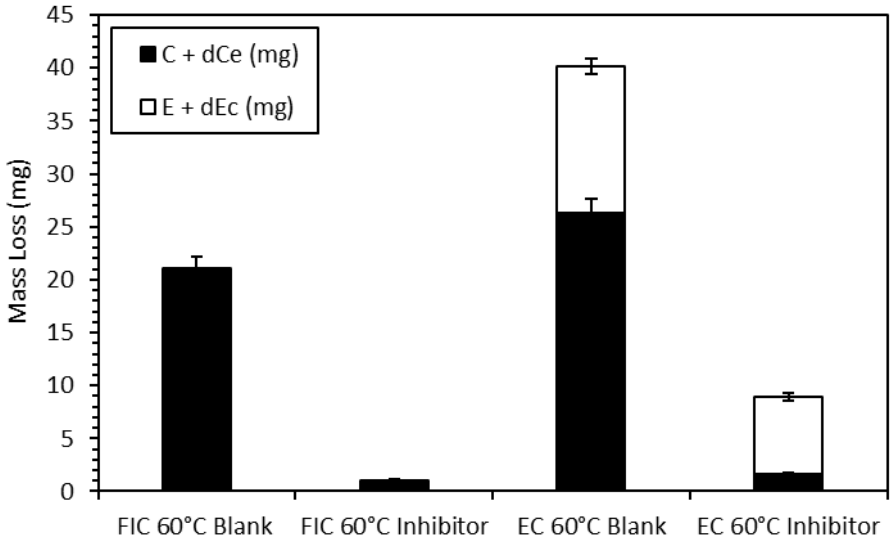

Figure 5: Contribution of erosion and corrosion components of degradation, drawing attention to the influence of the sand particles on inhibitor performance at 100 ppm.

FIC tests do not incorporate the erosion component (E + dEc), therefore the total mass loss (TML) is totally associated with flow induced corrosion, both in the presence and absence of the corrosion inhibitor. In these tests, it is noted that the use of 100 ppm of inhibitor was able to reduce the total degradation of material from 21.10 mg to 1.06 mg. In these tests, the total inhibitor efficiency is equivalent to electrochemical efficiency (95%).

In EC tests, it can be observed in blank tests conditions (0 ppm of inhibitor) that the process is dominated by corrosion ($C + dC_E$ = 26.28 mg), which represents almost 65% of the total degradation (TML = 40.15 mg) while erosion component (E + dEc = 13.87 mg) represents 35% of the total degradation (TML = 40.15 mg). With the use of 100 ppm of inhibitor, the percentage contribution of corrosion component ($C + dC_E$ = 1.69 mg) decreases to 19% while erosion component (E + dEc = 7.21 mg) increase to 81% of the total degradation (8.90 mg).

Furthermore, the use of inhibitor reduced the degradation attributed to the corrosion component ($C + dC_E$) from 26.28 mg to 1.69 mg, representing an electrochemical efficiency of inhibitor of 93.5%. Regarding the erosion component ($E + dE_C$), it can be observed that the use of the inhibitor reduced the mass loss from 13.87 mg to 7.21 mg, indicating the inhibitor efficiency in erosion was 48%. In addition, it can be observed that the use of the inhibitor was able to reduce the total degradation rate of erosion-corrosion from 40.15 mg to 8.90 mg, representing an inhibitor total efficiency of 78% of reduction. These efficiency parameters express the mitigation ability of the corrosion inhibitor acting on a wet ground surface of carbon steel at 60°C.

Some previous papers of Ramachandran *et al.* [14, 15, 26] suggest that several chemical inhibitors are capable of significantly reducing the corrosion component of damage induced by erosion/corrosion, but promote little or no resistance to pure erosion. However, other authors suggest that corrosion inhibitors have an effect on the erosion component and can reduce the total degradation to 50% [27]. In the present work, it was possible to observe that the use of inhibitor reduced the erosion component by 48%. An understanding of the mechanisms to support the development of efficient chemical products and adequate degradation control in these environments is essential. The hydrodynamic effect could present two effects on inhibition performances. First, it can increase the mass transport of inhibitor molecules to the steel surface improving the inhibitor efficiency. Second, the high shear stress resulted from high flow velocity can remove inhibitor layers from steel surface harming the inhibitor efficiency. This combined effect of both can result in a peak-value of inhibitor concentration at high flow velocities [16].

The efficiency results of inhibitor obtained at 60°C were compared to tests performed at 25°C [9]. Table 5 presents the electrochemical and total efficiency of corrosion inhibitor for these temperatures.

Table 5: Electrochemical and total efficiency of corrosion inhibitor after EC tests at 25 and 60°C

Inhibitor Efficiencies		Efficiency (%) versus Temperature (°C)	
		25°C [9]	60°C [current paper]
EC	Electrochemical	96%	93.5%
	Total	86%	78%

3.1.3. SURFACE ANALYSIS

In FIC tests, the total mass loss obtained after the tests is totally associated with uniform corrosion occurring on the sample surface. The calculation of the general thickness loss could be predicted using the corrosion rate obtained from *in situ* electrochemical tests. Figure 6 shows the general thickness loss and the wear zone created predominantly in the center of the sample of the specimens after FIC tests. SEM images of the centre of the specimens could also observed.

Figure 6 (a) and (c) show the profilometry analysis and it is noted the use of inhibitor was able to reduce the general thickness loss (5.5 μm to 0.3 μm) as well as the wear effect produced by the action of the hydrodynamic forces, making possible to observe the localised effect of the inhibitor.

The use of inhibitor is efficient to preventing the wear on surface when only flow reach the metal surface and it confirms the results obtained from LPR technique. Furthermore, it may be noted that the sample surface in the absence of corrosion inhibitor exhibits a significant wear and it is caracteristic of a uniform dissolution across the sample surface while in inhibited environments there is no wear caused by the flow evidencing a protection of the surface by the action in the inhibitor.

Regarding iron carbonate precipitation during the tests, that is not occur under experimental conditions and it is established in SEM images after the tests.

.

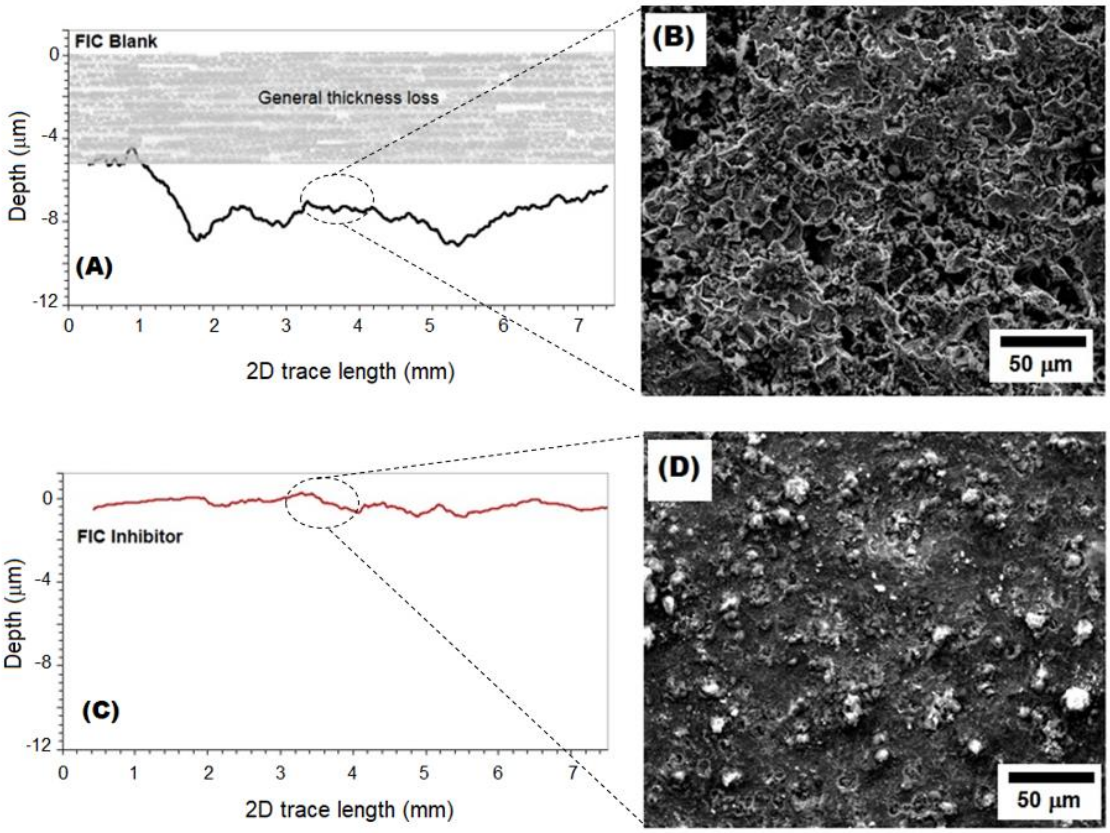

Figure 6: 2D surface profiles ((a) and (c)) and SEM images ((b) and (d)) of central region reached directly by the flow of the corrosion specimens after FIC tests in the absence and presence of corrosion inhibitor.

The surface profiles and SEM images of the centre of the samples after EC tests in the absence and presence of corrosion inhibitor are shown in Figure 7. Thickness loss was calculated using the corrosion rates obtained from *in situ* electrochemical tests and it was reduced from 6.8 μm (blank tests) to 0.3 μm (inhibited tests) and is represented in Figure 7 (a) and (c). Figure 7(a) presents a "W" shape and the highest erosion-corrosion depth occurs at the position about 6.5 mm of 2D trace length which is consistent with previous studies in similar conditions [28, 29, 30]. In the central region reached directly by the flow, the normal stress dominates the damage mechanism and there is direct impact of the sand particles on the material surface, forming an indentation morphology caused by plastic deformation. Also, there is a high static pressure in this region, causing a change of direction of the flow and it results in a higher drag force for solid particles [28].

The use of corrosion inhibitor reduces the maximum wear depth and indicates that the inhibitor presents a localised effect, i.e., in addition to reducing the total

degradation rate, it is able to reduce the maximum wear depth in the region directly affected by the solid particles. The effect of inhibitor on the reduction of the maximum wear depth (erosion-corrosion depth) can be observed by the profilometry result represented in Figure 7 (a) and (c).

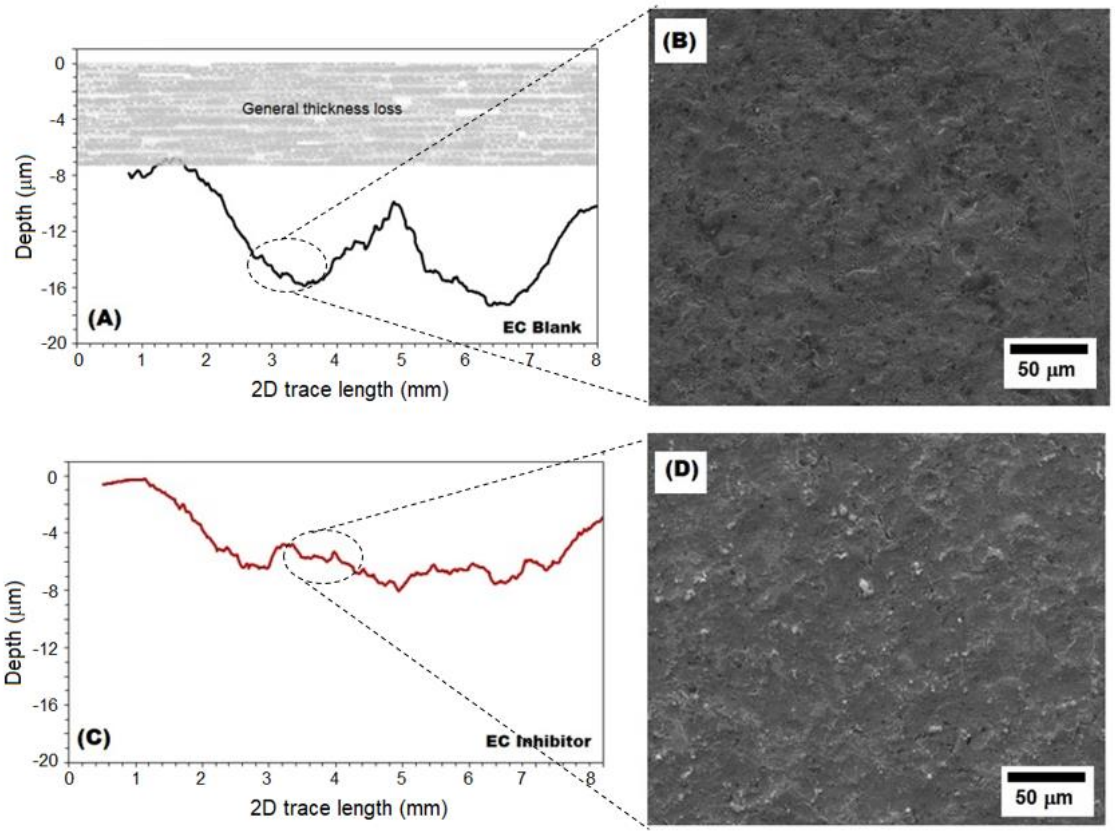

Figure 7: 2D surface profiles ((a) and (c)) and SEM images ((b) and (d)) of central region reached directly by the flow with solid particles of corrosion specimens after EC tests in the absence and presence of corrosion inhibitor.

SEM images (Figure 7 (b) and (d)) show the surface morphologies after EC tests, where plastic deformation caused by the impact of the sand particles on the region is observed. This image is commonly observed in samples subjected to EC tests when the particle incidence region is analysed [5, 10, 31]. In the absence of inhibitor, the adjacent area not directly reached by the sand particles exhibited uniform dissolution morphology, similar to the same region observed after FIC tests.

3.2 $FeCO_3$ PRE-FILMED X65 STEEL SPECIMENS – TEST CONDITIONS E, F, G, H.

3.2.1. PREVIOUS $FeCO_3$ FILM FORMATION

Figure 8 indicates the top view and cross-section of the developed $FeCO_3$ layer after to exposure to the CO_2-saturated 1.5 wt.% NaCl solution at 60ºC and 30 bar and pH adjusted to 6.6 in an autoclave during 48 hours. The average thickness was ~60µm. According to previous work [9], in similar conditions, there is a formation of homogeneous $FeCO_3$ layer, covering the entire surface.

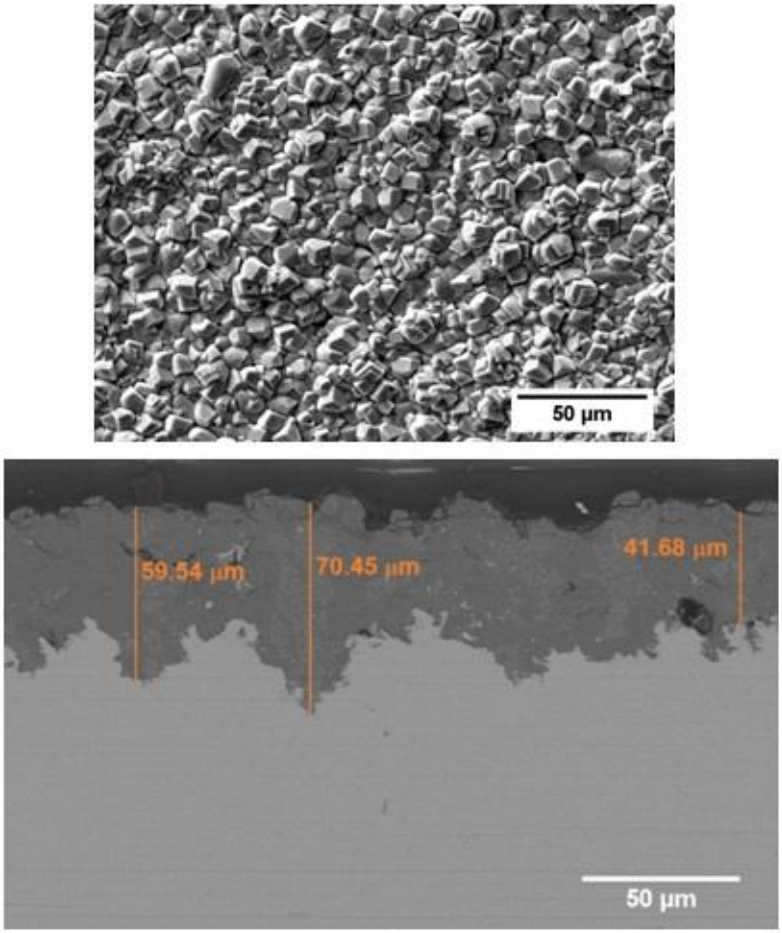

Figure 8: SEM images showing (a) top view and (b) cross-section view of the precipitated $FeCO_3$ layer on X65 steel surface after exposure in a CO_2-saturated 1.5wt.% NaCl brine at 60ºC and 30 bar for 48 h.

3.2.2. ELECTROCHEMICAL RESULTS

3.2.2.1. $FeCO_3$ FILM STABILITY

Some long-term static tests in 3.5% NaCl solution at 60°C were performed and electrochemical corrosion rate was measured during 45 hours in order to verify the corrosion behaviour, evaluate the stability of $FeCO_3$ film and its possible interference in the inhibitor performance without hydrodynamic conditions.

Figure 9 shows the corrosion rate values for blank and pre-filmed tests in the absence and presence of corrosion inhibitor for long-term static tests. Blank tests presented constant values around 3 mm/year during entire test. Table 6 presents the Stern-Geary coefficients (B) applied for the calculation of corrosion rate using the LPR data.

Pre-filmed samples in uninhibited environments presented an increase in electrochemical corrosion rate, reaching values close to obtained in blank tests after 45 hours. However, in the first two hours the values are lower than 0.5 mm/year and in the operation window of SIJ, the corrosion rate is 0.8 mm/year. From this point, it is possible to observe a fast increase in the corrosion rate, reaching values close to blank tests and indicating that the $FeCO_3$ film tends to lose its protective characteristic after long hours.

Pre-filmed samples in inhibited environments showed a corrosion rate close to 0.11 mm/year during throughout the experiment. In this case, this value of corrosion rate is higher than when only the corrosion inhibitor is used in the system, indicating that part of the film can remain on the steel surface, not promoting protection and disrupting the individual action of the inhibitor.

In long-term tests, the fact of coexistence film + inhibitor do not mean that the protection will be better. Because it will depend on the action of inhibitor on the metal surface. Part of the film can remain on the steel surface, not promoting protection and disrupting the individual action of the inhibitor. The higher efficiency of the corrosion inhibitor on grinded surface when compared with $FeCO_3$ rich interface is not unexpected and not even surprising. The direct access of the inhibitor to the steel surface is possible without the interference of the precipitated film and hence the inhibiting action is favored. Another point is the increase of the specific surface area promoted by the presence of the porous precipitate film. The positive contribution of the corrosion inhibitor is expected on areas of the steel directly exposed to the corrosion environment. The hypothesis of a synergistic effect between precipitated film and corrosion inhibitors cannot be confirmed.

Table 6: Stern-Geary coefficients used in long-term static tests

	Blank Static	Inhibitor Static	$FeCO_3$ film Static	$FeCO_3$ film + inhibitor Static
βa (mV/decade)	82	65	66	48
βc (mV/decade)	122	305	210	250

Stern-Geary coefficient (B) mV/decade	21.31	23.27	21.71	17.37

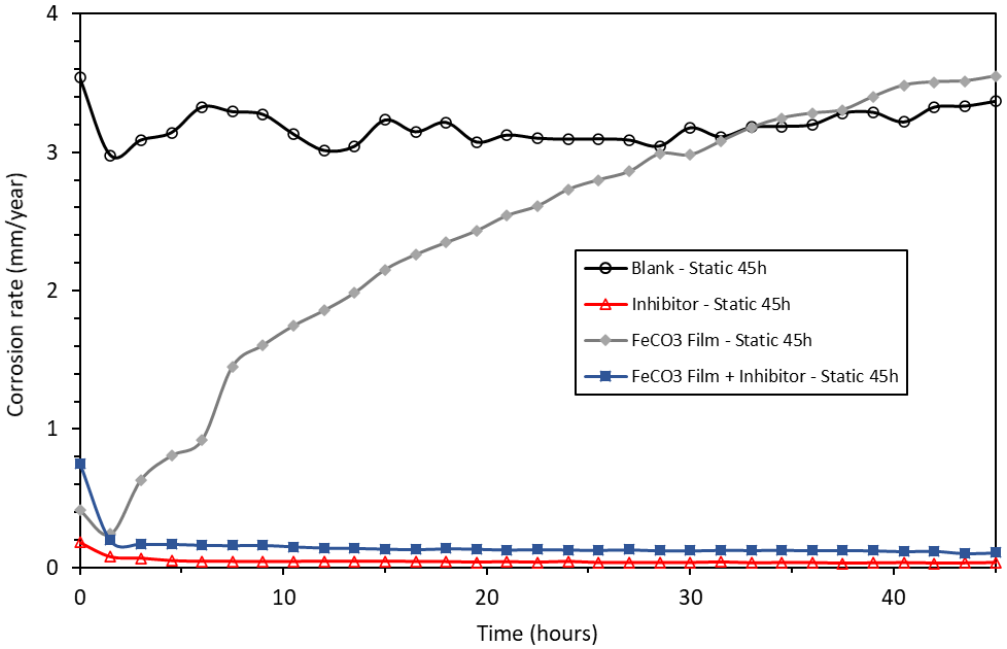

Figure 9: Corrosion rates obtained from LPR measurements in the absence and presence of FeCO3 film and corrosion inhibitor Test conditions: Static Tests, 60°C, NaCl 3,5%, pH 3.8, 48h.

3.2.2.2. FIC AND EC TESTS

FIC and EC tests were performed on specimens after the pre formation $FeCO_3$ on the steel surface. Table 7 presents the Stern-Geary coefficients (B) applied for the calculation of corrosion rate using the LPR data. The analysis of LPR results and its representation could be seen in Figure 10 and 11, which compares the corrosion rates under FIC and EC conditions with and without corrosion inhibitor at 60°C.

Table 7: Stern-Geary coefficients used in Flow Induced Corrosion and Erosion Corrosion tests.

	FIC 60°C Blank	FIC 60°C Film	FIC 60°C Inhibitor + Film	EC 60°C Blank	EC 60ºC Film	EC 60ºC Inhibitor + Film
βa (mV/decade)	100	66	48	101	59	63

βc (mV/decade)	126	210	250	128	205	280
Stern-Geary coefficient (B) mV/decade	23.17	21.71	17.37	24.45	19.81	22.35

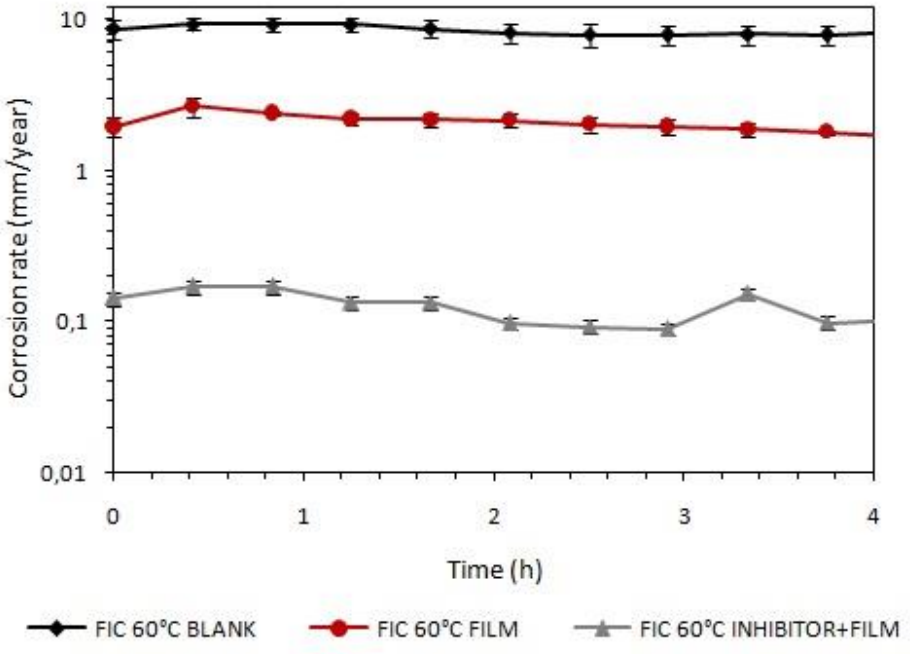

Figure 10: Corrosion rates obtained from LPR measurements during FIC tests with and without corrosion inhibitor on X65 steel specimens (wet-ground or initially pre-filmed with $FeCO_3$)

The sole presence of $FeCO_3$ film is able to reduce the flow induced corrosion rate from 8.0 to 1.81 mm/year representing a protection ability of the film of 77%. The corrosion rate remains constant during entire test and the $FeCO_3$ film could remain on the surface of the steel and ensures a significant protection efficiency. The persistence of the $FeCO_3$ film at 60°C was confirmed by the results obtained from the static tests where corrosion rate was 0.8 mm/year in the operation window of SIJ.

The presence of $FeCO_3$ film and inhibitor simultaneously under FIC conditions lowered the corrosion rate from 8.0 mm/year to 0.11 mm/year and the electrochemical efficiency achieved was 98.7%, slightly higher the results achieved with the only presence of the film. These results indicate that both alternatives, use of corrosion inhibitor and $FeCO_3$ precipitation, have the ability to mitigate the CO_2 corrosion process even under the influence of the flow at 60°C. The use of the inhibitors emerges as an

efficient protection technology for carbon steel in case of incomplete formation of $FeCO_3$ on the metallic surface.

Table 8 presents a comparison of the corrosion rates obtained at 25 [9] and 60°C after FIC tests on wet-ground (blank) and $FeCO_3$ pre-filmed with and without inhibitor.

At 25°C [9], the sole presence of $FeCO_3$ was able to reduce the corrosion rate from 4.9 mm/year to 0.2 mm/year representing an electrochemical efficiency of 96% and it is slightly higher the results achieved at 60°C (77%). Furthermore, the addition of the corrosion inhibitor when the $FeCO_3$ is already present reduces the corrosion rate further to 0.07 mm/year at 25°C [9] while it is 0.11 at 60°C, respectively. It represents an electrochemical efficiency of 98.6% for both, when compared to blank tests in each temperature. However, it is important to investigate the surface obtained from SEM analysis to identify whether this electrochemical protection is associated to $FeCO_3$ film, inhibitor or both.

Table 8: Summary of corrosion rates from LPR after FIC tests on wet-ground or initially pre-filmed with $FeCO_3$ with and without corrosion inhibitor at 25 [9] and 60°C

Test conditions		Corrosion rate (mm/year) versus Temperature (°C)	
		25°C [9]	60°C [current paper]
FIC	0 ppm inhibitor No $FeCO_3$ film (Blank)	4.9	8.0
	No inhibitor Presence of $FeCO_3$ film (Film)	0.2	1.81
	100 ppm inhibitor Presence of $FeCO_3$ film (Inhibitor + Film)	0.07	0.11

Another scenario was investigated, in the presence of solid particles in the corrosive environment simulating erosion-corrosion tests. Figure 11 shows the LPR corrosion rates obtained for pre-filmed samples, both in the absence and presence of corrosion inhibitor compared to blank tests in EC conditions.

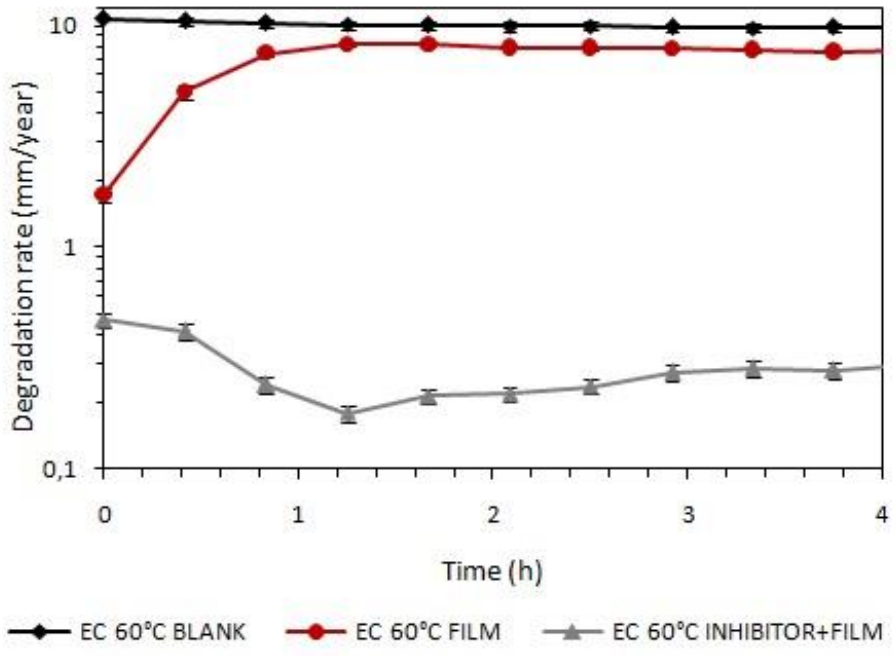

Figure 11: Corrosion rates obtained from LPR measurements during EC tests with and without corrosion inhibitor on X65 steel specimens (wet-ground or initially pre-filmed with $FeCO_3$)

The presence of sand in the system aggravates the deterioration conditions, since in addition to the electrochemical corrosion there is a mechanical erosion on the steel surface. The corrosion rate of the pre-filmed samples increases rapidly reaching values close to the values obtained from blank tests (9.9 mm/year) after 1 hour. This result suggests the mechanical removal of the $FeCO_3$ film in the region of direct impact of the sand particles. These successive impacts of solid particles against the steel surface prevents the protective film from forming again in that region, leaving the steel surface exposed to the corrosive environment. Precipitation of $FeCO_3$ is not likely to occur under the experimental conditions, due to the high V/A ratio, where V is the volume of solution and A is the total area of steel exposed to the environment. $FeCO_3$ precipitation depends on the increment of the concentration of iron ions in solution. The results of surface analysis of the steel samples tested on wet ground surface conditions support this assumption.

It is important to highlight that corrosion product layer and inhibitor film are fully affected by the flow velocity and presence of sand particles. The impact of these particles on metal surface can promote a local stresses very high and the high velocity sand can degraded the corrosion product layer. In addition, some inhibitor molecules can be removed from metal surface by the flow and sand particles impinged metal surface [16].

However, it was observed that the combination of the use of inhibitor and the presence of $FeCO_3$ film on the surface was able to keep the corrosion rate in very low values, closes to 0.3 mm/year, corresponding to an electrochemical efficiency of protection of 97%, a significant reduction of the corrosion rate compared to the blank test (9.9 mm/year).

Table 9 presents a summary of the corrosion rates in EC tests at 25°C [9] and 60°C, obtained by LPR technique of initially pre-filmed with $FeCO_3$ samples in the presence and absence of inhibitor. It can be concluded that the use of corrosion inhibitor in pre-filmed samples significantly reduces the corrosion rate when compared to the isolated effect of $FeCO_3$ precipitation (from 8.21 to 0.31 mm/year) at 60°C. This effect could indicate that the corrosion inhibitor would compensate the local increase of the degradation produced where the $FeCO_3$ layer is removed by the direct impact of the sand particles. In other words, the central region in the sample that would have the substrate exposed to the corrosive environment would receive protection by the action of the inhibitor. In addition, the inhibitor may be acting in conjunction with the $FeCO_3$ layer outside of this central region and thus improving the protection of the surface against the corrosive process. As shown in FIC tests, the effect of the joint action between the $FeCO_3$ layer and the inhibitor can be observed by the slightly higher efficiency obtained when only the corrosion inhibitor is used (Figure 4). However, the possible interference of the inhibitor on the $FeCO_3$ film formation process should be further investigated.

However, when these results are compared to results obtained at 25°C in the previous work [9], it is possible to identify that sole presence of $FeCO_3$ film is able to protect the surface even with the presence of solid particles only in lower temperatures. The sole presence of $FeCO_3$ reduces the electrochemical corrosion rate from 5.5 mm/year to 0.7 mm/year at 25°C [9] representing an electrochemical efficiency of 87% while it is not effective at 60°C.

The addition of the corrosion inhibitor when the $FeCO_3$ is already present decreases the electrochemical corrosion rate further 0.7 mm/year to 0.1 mm/year at 25°C [9] and it represents an efficiency of 98,2%. In the same condition at 60°C, it is possible to observe an efficiency of 97% compared to blank tests. However, as mentioned in FIC tests, it is important to investigate the surface obtained from SEM analysis to identify whether this electrochemical protection is associated to $FeCO_3$ film, inhibitor or both.

Table 9: Summary of corrosion rates from LPR after EC tests on pre-filmed samples with and without corrosion inhibitor at 25°C [9] and 60°C

Test conditions		Corrosion rate (mm/year) versus Temperature (°C)	
		25°C [9]	60°C [current paper]
EC	0 ppm inhibitor No $FeCO_3$ film (Blank)	5.5	9.90
	No inhibitor Presence of $FeCO_3$ film (Film)	0.7	8.21
	100 ppm inhibitor Presence of $FeCO_3$ film (Inhibitor + Film)	0.1	0.31

3.2.3. TOTAL DEGRADATION RATE

In addition to the electrochemical analysis, it is known that in the EC condition it is also necessary to consider the erosive effect caused by the impact of the sand particles. Table 10 and Figure 12 show the Total Mass Loss (TML), the corrosion (C + dCe) and erosion (E + dEc) components for initially pre-filmed with $FeCO_3$ samples after FIC and EC tests. For the calculation of the total degradation rate of pre-filmed samples it was used the mass after the $FeCO_3$ film formation and after the SIJ tests. Then, Figure 11 represents the effect of erosion and corrosion components on the film and substrate.

FIC tests do not have an erosion component related and the total mass loss (TML) is totally associated with flow-induced corrosion, both in the presence and absence of the corrosion inhibitor. In these tests, it is noted that the use of the inhibitor and $FeCO_3$ film was able to reduce the total degradation from 4.8 mg to 0.3 mg when compared to sole presence of $FeCO_3$.

In EC tests, without the presence of inhibitor, the contribution of corrosion (C + dCE = 21 mg) and erosion (E + dEc = 17 mg) components is almost equal, representing 55% and 45% of total degradation (38 mg) of material, respectively. With the addition of 100ppm of inhibitor into the system, the percentage contribution of corrosion component ($C + dC_E$ = 0.8 mg) is 10% while erosion component (E + dEc = 7.2 mg) represents 90% of the total degradation (8.0 mg). This effect could be associated to the protection promoted by the action of inhibitor in the region where $FeCO_3$ layer was removed by the direct impact of the particles.

Table 10: Mass loss associated to corrosion and erosion components

Test conditions		Mass loss (mg) associated to components of degradation		
		C + dCe	E + dEc	TML
FIC	No inhibitor Presence of $FeCO_3$ film (Film)	4.8	-	4.8
	100 ppm inhibitor Presence of $FeCO_3$ film (Inhibitor + Film)	0.3	-	0.3
EC	No inhibitor Presence of $FeCO_3$ film (Film)	21	17	38
	100 ppm inhibitor Presence of $FeCO_3$ film (Inhibitor + Film)	0.8	7.2	8.0

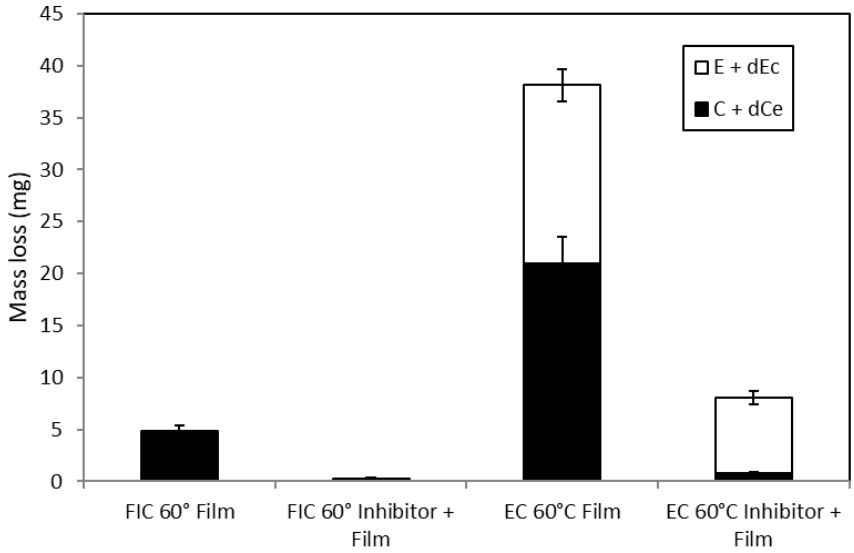

Figure 12: Contribution of erosion and corrosion components of degradation, drawing attention to the influence of the sand concentration on $FeCO_3$ film and inhibitor performance at 100 ppm.

3.2.4. SURFACE ANALYSIS

Figure 13 shows the surface profiles and SEM images after FIC tests in the absence and presence of $FeCO_3$ film and corrosion inhibitors.

It can observe that the specimen has not presented a central region with wear scar both the presence and absence of the inhibitor. The sample with only $FeCO_3$ film showed a high surface roughness along the entire surface, indicating a general corrosion that would cause a greater degradation because with a possible dissolution of the film the substrate would be more exposed to the corrosive environment. These results are confirmed by SEM images of uninhibited tests (Figures 13b), the $FeCO_3$ film does not remain integrally on the central region of the sample, which exhibits high degradation. It is not clear whether this degradation was the effect of the chemical dissolution or result of the hydrodynamic forces present due to the turbulent flow effects. However, the corrosion rates of these tests presented lower values than in the blank, about 77% lower.

In the presence of pre-filmed samples and inhibitor, it is observed that the surface presents almost no wear and surface roughness, and that probably the $FeCO_3$ film is maintained, because the values of corrosion rate from LPR were smaller than when only the inhibitor was used. From the surface analysis obtained by SEM (Figure 13d) it was possible to observe the persistence of the film in entire sample surface after FIC tests. It is possible to observe that the grains of the $FeCO_3$ film remain uniformly under the surface of the steel. Thus, it was observed that the corrosion rate of this sample was about 94% lower than when only the $FeCO_3$ film was used (1.81 mm/year to 0.1 mm/year – Table 8). In addition, without the presence of sand, it can be concluded that the $FeCO_3$ film acts in conjunction with the inhibitor, adding a surface protection, which acts as a diffusion barrier of cathodic species as well as covering the steel surface and blocking the reaction of dissolution of iron.

This result is still in agreement with the wear profile obtained for this sample. In Figure 13, it can be seen that the use of the inhibitor maintains the surface of the sample with a lower surface roughness than when only the $FeCO_3$ film was used. This suggests that the inhibitor is capable of improving the resistance of the $FeCO_3$ layer to hydrodynamic removal, chemical dissolution or both [9].

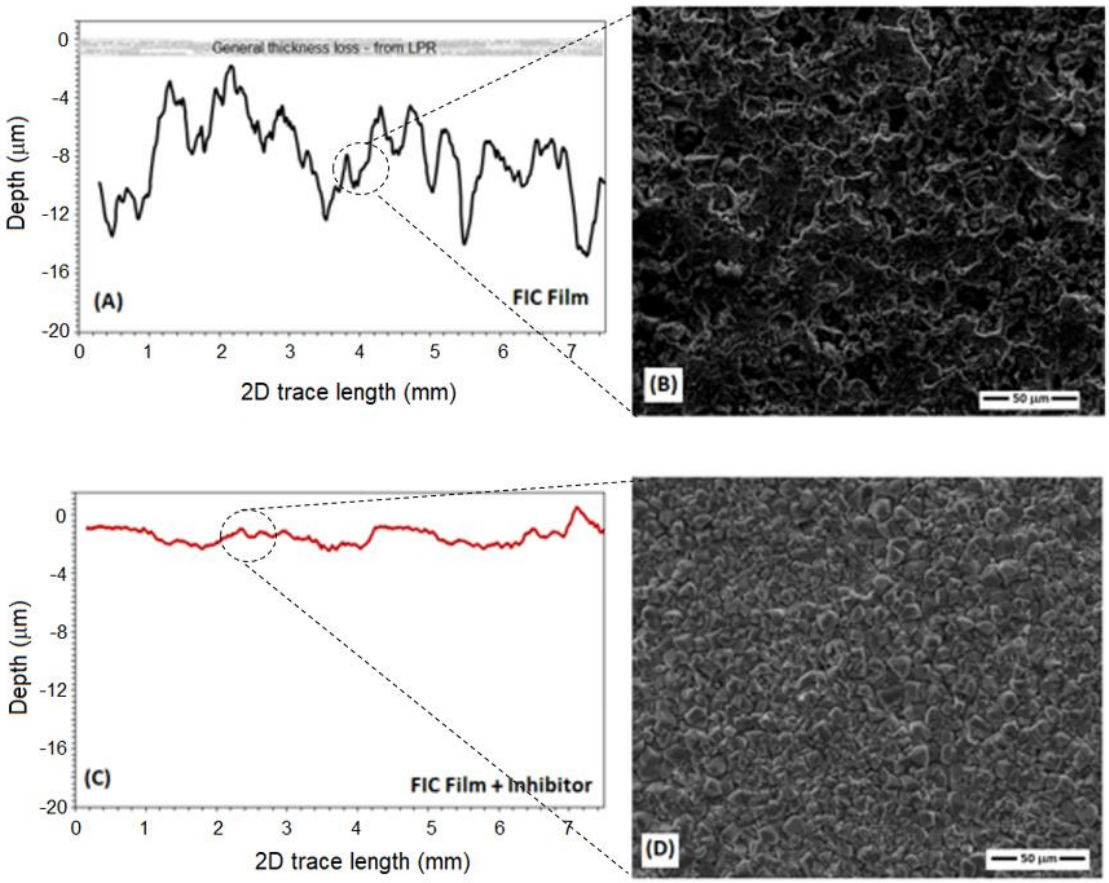

Figure 13: 2D surface profiles ((a) and (c)) and SEM images ((b) and (d)) of central region reached directly by the flow of previously $FeCO_3$ pre-filmed specimens after FIC tests in the absence and presence of corrosion inhibitor.

With the introduction of solid particles into the system it is possible to observe a wear scar in the central region of the sample both with the use of $FeCO_3$ film and the film and inhibitor together. Figure 14 shows the total penetration depth of wear scar and surface morphologies of pre-filmed samples after the EC tests at 60°C, in the absence and presence of corrosion inhibitor.

Pre-filmed samples in uninhibited environments (Figure 14b) presented a steel surface with no $FeCO_3$ film which was removed by the presence of sand. This confirms the data obtained in the profile analysis of the sample which it can be observed that in the central region of the wear scar close to 45 µm, Figure 14a. However, this depth is related to both the loss of film thickness and the substrate, so it is not possible to know exactly how much film remains on the surface. Furthermore, it is not possible to observe a plastic deformation in this region, as previously observed for the samples after blank tests (with no $FeCO_3$ film and inhibitor), Figure 7b.

When the inhibitor is added to the system (Figure 14 (c)), it is noted that the maximum depth of wear scar decreases to values close to 20μm, reducing by half when compared to the use of the film alone. However, it does not prevent the partial removal of the film by the sand particles in the central region of the sample, Figure 14d.

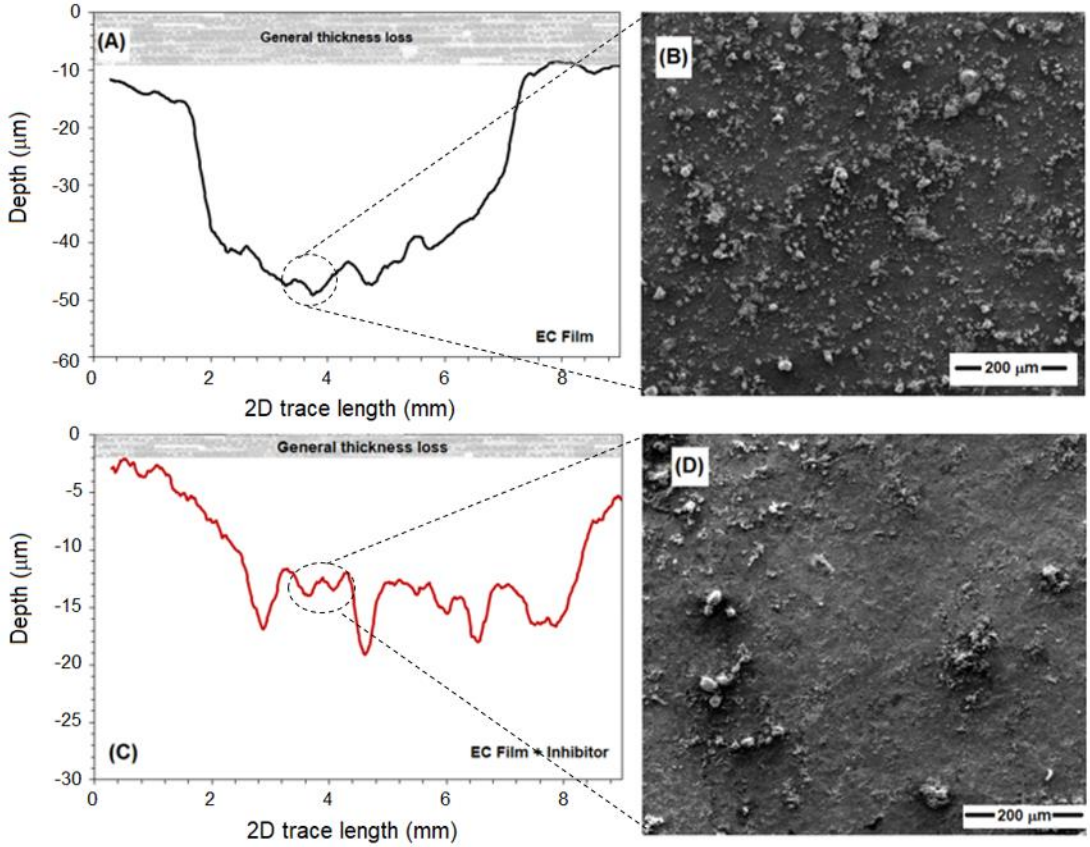

Figure 14: 2D surface profiles and SEM images of previously $FeCO_3$ pre-filmed X65 steel specimens after EC tests in the absence and presence of corrosion inhibitor.

Towards the outer edge of the material surface, Figure 15, it is possible to observe the presence of corrosion inhibitor on the FeCO3 film causing an impact on the fraction of corrosion inhibitor concentration available to act on the exposed steel surface. In addition, part of FeCO3 layer could be restricting the mass transfer of reactants and products between the bulk solution and this region of the metal surface. As a result, the reduction of cumulative mass loss in the presence of inhibitor could be explained by surface morphology characters of the corrosion product layer [16].

According to López et al. (2005) [32], some inhibitors are capable of incorporate into the corrosion product and provide a protective barrier against the corrosive environment.

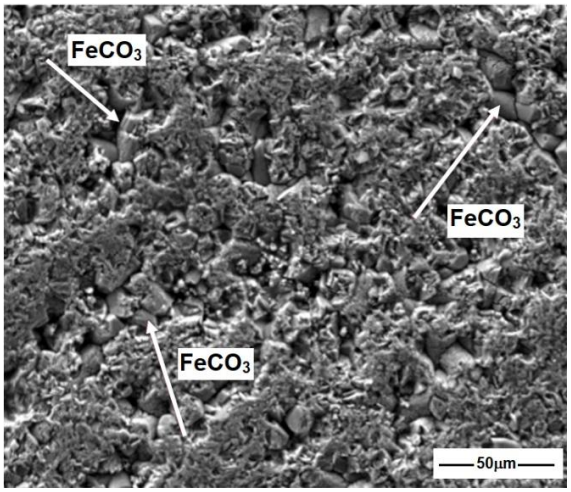

Figure 15: SEM images indicating contour area in the presence of corrosion inhibitor and FeCO3 layer after EC tests (1000mg/L sand).

4 CONCLUSIONS

The $FeCO_3$ layer preformed on the steel surface was evaluated in CO_2-containing FIC and EC environment at 60°C, both in the absence and presence of corrosion inhibitor. From this study, the following can be concluded:

- The use of corrosion inhibitor reduced the corrosion rates values to approximately 0.5 mm/year both in the absence and presence of solid particles at 60°C. This represented an inhibitor efficiency of 95% in relation to the electrochemical corrosion component damage and it is similar to obtained at 25°C [9] and it indicate the inhibition action is maintained whether higher temperature.

- Total degradation rate of EC for X65 carbon steel was reduced by 78% in the presence of sand through the addition of 100 ppm inhibitor at 60°C and it is slightly lower than the results achieved at 25°C [9].

- The sole presence of the $FeCO_3$ layer on the steel surface was able to reduce the corrosion rate in uninhibited environments by 77%. However, with the addition of solid particles, the $FeCO_3$ layer was not sufficient to attenuate the corrosive process, promoting a rapid increase in the corrosion rate to values similar to tests in the absence of the corrosion product.

- The application of corrosion inhibitor in conjunction with pre-filmed test specimen reduced the corrosion rate component of total degradation further in comparison to the effect observed in the presence of only the $FeCO_3$. This effect was significant in both the absence and presence of sand, representing a synergistic effect between the $FeCO_3$ layer and the corrosion inhibitor.

- The application of inhibitor did not prevent $FeCO_3$ layer removal by the sand particles in the central region of the sample. However, at the edge of the sample it appeared that the $FeCO_3$ had become more durable due to integrate of the inhibitor with the film.

5 ACKNOWLEDGEMENTS

The authors would like to acknowledge the support provided by CNPq, ANP and Shell. In addition, we would like to thank Professor Eduardo Moreira da Silva of Fluminense Federal University for help with carrying out the 2D profile measurements.

6 REFERENCES

[1] T. Li, Y. Yang, K. Gao, M. Lu, Mechanism of Protective Film Formation during CO_2 Corrosion of X65 Pipeline Steel. Journal of University of Science and Technology Beijing, Mineral, Metallurgy, Material 15 (2008) 702-706.

[2] M.B. Kermani, A. Morsed, Carbon dioxide corrosion in oil and gas production: A compendium, Corrosion, 59 (8) (2003) 659-683.

[3] Z.B. Zheng, Y.G.Zheng, Effects of surface treatments on the corrosion and erosion-corrosion of 304 stainless steel in 3.5% NaCl solution, Corrosion Science 112 (2016) 657-668.

[4] M. Parsi, K. Najmi, F. Najafifard, S. Hassani, B. S.McLaury, S. A. Shirazi, A comprehensive review of solid particle erosion modelling for oil and gas wells and pipelines applications, Journal of Natural Gas Science and Engineering 21 (2014) 850-873.

[5] R. Barker, A. Neville, X. Hu, S. Cushnaghan, Evaluating inhibitor performance in CO2-saturated erosion-corrosion environments, Corrosion 71 (1) (2015) 14–29.

[6] X. Hu, R. Barker, A. Neville, A. Gnanavelu, Case study on erosion-corrosion degradation of pipework located on an offshore oil and gas facility, Wear 271 (2011) 1295–1301.

[7] A. Akbar, X. Hu, C. Wang, A. Neville, The Influence of Flow Rate, Sand and Inhibitor on Iron Carbonate Scales under Erosion-corrosion Conditions using a Submerged Impingement Jet, NACE Corros (PAPER ID: NACE-2012–1396), 2012.

[8] X. Hu, K.A. Raheem, A. Neville, A. Akbar, Effect of Different Types of Corrosion Films Formed in CO_2 Saturated Conditions on the In-Situ Corrosion of X65 Pipeline Steel Under Liquid-Solid Impingement, NACE Corros (PAPER ID:NACE- 2013-2188), 2013.

[9] E.V. Senatore, W. Taleb, J. Owen, Y. Hua, J.A.C. Ponciano Gomes, R. Barker, A. Neville, Evaluation of high shear inhibitor performance in CO_2-containing flow induced corrosion and erosion-corrosion environments in the presence and absence of iron carbonate films, Wear 404-405 (2018) 143-152.

[10] J. Owen, C. Ramsey, R. Barker, A. Neville, Erosion-corrosion interactions of X65 carbon steel in aqueous CO_2 environments, Wear 414-415 (2018) 376-389.

[11] Md. A. Islam, Z. Farhat, Erosion-corrosion mechanism and comparison of erosion-corrosion performance of API steels, Wear 376-377 (Part A) (2017) 533-541.

[12] S. Hassani, K.P. Roberts, S. Shirazi, J. R. Shadley, E. F. Rybicki, C. Joia, A New Approach for Predicting Inhibited Erosion-Corrosion in CO_2- saturated oil/brine Flow Condition, SPE International Conference & Workshop on Oilfield Corrosion (PAPER ID: SPE-155136-PA), 2012.

[13] A. Neville, C. Wang, Erosion-corrosion mitigation by corrosion inhibitors – an assessment of mechanisms, Wear 267 (2009) 195–203.

[14] S. Ramachandran, K.A. Bartrip, C. Menendez, S. Coscio, Preventing Erosion and Erosion Corrosion using specialty chemicals, SPE International Conference & Workshop on Oilfield Corrosion (PAPER ID: SPE-80218-MS), 2003.

[15] S. Ramachandran, Y.S. Ahn, V. Jovancicevic, J. Basset, Further Advances in the Development of Erosion Corrosion Inhibitors, NACE Corros (PAPER ID: NACE05292), 2005.

[16] X. Jiang, Y.G. Zheng, W. Ke, Effect of flow velocity and entrained sand on inhibition performances of two inhibitors for CO2 corrosion of N80 steel in 3% NaCl solution, Corrosion Science 47 (2005) 2636-2658.

[17] M. Nordsveen, S. Nesic, A Mechanistic Model for Carbon Dioxide Corrosion of Mild Steel in the Presence of Protective Iron Carbonate Films – Part 2: A Numerical Experiment, NACE Corros (PAPER ID: NACE-03060489), 2003.

[18] A. Dugstad, Mechanism of Protective Film Formation During CO_2 Corrosion of Carbon Steel, NACE Corros (PAPER ID: NACE-98031), 1998.

[19] G.H. Al-Aithan, F.M. Al-Mutahar, J.R. Shadley, S.A. Shirazi, E.F. Rybick, K.P. Roberts, A Mechanistic ErosionCorrosion Model for Predicting Iron Carbonate ($FeCO_3$) Scale Thickness in a CO_2 environment with sand, NACE Corros (PAPER ID: NACE-2014-3854), 2014

[20] A. S. Nassef, N. Banazadeh-Neishabouri, M. W. Keller, K. P. Roberts, E. F.Rybicki, E. V. Iski, S. A. Shirazi, Comparison of Erosion Resistance of Iron Carbonate Protective Layer with Calcium Carbonate Particles Versus Sand, SPE International Conference & Workshop on Oilfield Corrosion (PAPER ID: SPE-188531-MS), 2017.

[21] K. Choksi, W. Sun, S. Nesic, Iron Carbonate Scale Growth and the Effect of Inhibition in CO2 Corrosion of Mild Steel, NACE Corrosion (PAPER ID NACE-05285), 2005.

[22] ASTM G31-72(1999), Standard Practice for Laboratory Immersion Corrosion Testing of Metals, ASTM International, West Conshohocken, PA, 1999.

[23] ASTM G102-89(2010), Standard Practice for Calculation of Corrosion Rates and Related Information from Electrochemical Measurements, ASTM International, West Conshohocken, PA, 2010.

[24] S. Nesic, Key issues related to modelling of internal corrosion oil and gas pipelines – A review, Corrosion Science 49 (12) (2007) 4308-4338.

[25] M. M. Stack, S. M. Abdelrahman, B. D. Jana, Some perspectives on modelling the effect of temperature on the erosion–corrosion of Fe in aqueous conditions, Tribology International 43 (12) (2010) 2279-2297.

[26] S. Ramachandran, M. B. Ward, K. A. Bartrip, V. Jovancicevic, Inhibition of the Effects of Particle Impingement, NACE Corrosion (PAPER ID: NACE-02498), 2002.

[27] X. Hu, K. Alzawai, A. Gnanavelu, A. Neville, C. Wang, A. Crossland, J. Martin, Assessing the effect of corrosion inhibitor on erosion–corrosion of API-5L-X65 in multi-phase jet impingement conditions, Wear 271 (9–10) (2011) 1432-1437.

[28] J.Z. Yi, H.X. Hu, Z.B. Wang, Y.G. Zheng, On the critical flow velocity for erosion-corrosion in local eroded regions under liquid-solid jet impingement, Wear 422-423 (2019) 94-99.

[29] A. Gnanavelu, N. Kapur, A. Neville, J.F. Flores, An integrated methodology for predicting material wear rates due to erosion, Wear 267 (2009) 1935-1944.

[30] J. Yao, F. Zhou, Y.L. Zhao, H. Yin, N. Li, Investigation of erosion of stainless steel by two-phase jet impingement, Applied Thermal Engineering 88 (2015) 353-362.

[31] W. Zhao, C. Wang, T. Zhang, M. Yang, B. Han, A. Neville. Effects of laser surface melting on erosion–corrosion of X65 steel in liquid–solid jet impingement conditions, Wear 362–363 (2016) 39-52.

[32] D.A. López, S. N. Simison, S. R. de Sánchez, Inhibitors Performance in CO_2 Corrosion: EIS Studies on the Interaction between their Molecular Structure and Steel Microstructure, Corrosion Science 47 (3) (2005) 735-755.